Results in Materials 11 (2021) 100207

Contents lists available at ScienceDirect

Results in Materials

journal homepage: www.sciencedirect.com/journal/results-in-materials

High-speed machining tool-steel chips as an outstanding raw material for indirect additive manufacturing?

R.F. Santos [a,b,*], A.R. Farinha [c], R. Rocha [d], C. Batista [e], G. Costa Rodrigues [f], M.T. Vieira [c]

[a] Department of Metallurgical and Materials Engineering, University of Porto, Rua Dr. Roberto Frias, 4200-465 Porto, Portugal
[b] LAETA/INEGI – Institute of Science and Innovation in Mechanical and Industrial Engineering, Rua Dr. Roberto Frias, 4200-465 Porto, Portugal
[c] CEMMPRE – Centre for Mechanical Engineering, Materials and Processes, University of Coimbra, Rua Luís Reis dos Santos, 3030-788 Coimbra, Portugal
[d] CEMUP – Materials Centre of the University of Porto, Rua do Campo Alegre 823, 4150-180 Porto, Portugal
[e] CDRSP – Centre for Rapid and Sustainable Product Development, Polytechnic Institute of Leiria, Rua General Norton de Matos, Apartado 4133, 2411-901 Leiria, Portugal
[f] Adira Metal Forming Solutions, SA, Portugal

ARTICLE INFO

Keywords:
Tool-steel chip
Grain-refinement
Nanocrystalline
t-EBSD
Additive manufacturing

ABSTRACT

Sustainable recycling approaches are emerging topics for environmental safety of manufacturing technologies. Chips generated in high–speed machining (HSM) of as-quenched steels have a potential re-use for more sustainable and cost-efficient manufacturing routes, such as powder production from chip milling for additive manufacturing (AM). The objective of this study was to characterise tool-steel chips generated by HSM of an AISI-SAE H13 as-quenched workpiece and evaluate their potential use for powder production, as an alternative process to atomisation. Microhardness tests reveal that this type of waste has a suitable hardness for milling, which could be attributed to its microstructure. Chips were also analysed by X-ray diffraction, scanning and transmission electron microscopies, and transmission electron backscattering diffraction (t-EBSD) mapping. The microstructure of the areas adjacent to the adiabatic shear band (ASB), where intense material flow takes place, consists of thin martensite laths with high dislocation density and low angle grain boundaries (LAGB) or sub-grain regions. ASB consists of ultrafine and nanocrystalline grains. The results provide new insight on the grain-refining mechanism assisted by progressive martensite lath subdivision into small and near-equiaxed grains, as a direct result of intense strain accumulation and recrystallisation, endorsing HSM tool-steel chips as superior (nanocrystalline) and low-cost raw material for powder production.

1. Introduction

High-speed machining (HSM) is of great contribute for subtractive processes in the mould manufacturing industry, where the surface hardness is the main target. Machining hard steels contribute to avoiding subsequent heat treatments after machining and finishing stages, required to attain the desired hardness. The heat treatment of quenching after shaping is a source of stresses, dimensional variations and distortions, which constitute the main cause of failure during die/mould fabrication. The new subtractive and finishing processing by a high-speed rotating tool, with bits of a very hard material at the tip, forces the extraction of highly-strained metallic fragments — chips. These particles display smaller dimensions and higher hardness than the chips resulting from the cutting of annealed tool-steel by conventional processes. In opposition to conventional (low-speed) machining, HSM is especially suitable for quenched tool-steel dies/moulds [1]. In general, chips generated by machining procedures are treated as metal scrap and dispatched for smelting, which completely eliminates their processing history. A recent study [2] followed a replicative process approach to fabricate cylinders by compressing AISI-SAE H11 tool-steel conventional chips, previously converted into coarse powders. Effectively, instead of following a thermomechanical route, metallic chips could be raw materials for powder technology such as additive manufacturing (AM). AM is an umbrella concept for an emerging wide range of manufacturing methods based on the processing of powders to build parts/components layer by layer. Therefore, in order to take full advantage of the properties expected from the chips generated by HSM, it is of utmost importance to recycle them in the solid state, by means of AM indirect

* Corresponding author. LAETA/INEGI – Institute of Science and Innovation in Mechanical and Industrial Engineering, Rua Dr. Roberto Frias, 4200-465 Porto, Portugal.
E-mail address: rbns@fe.up.pt (R.F. Santos).

https://doi.org/10.1016/j.rinma.2021.100207
Received 27 April 2021; Received in revised form 1 June 2021; Accepted 2 July 2021
Available online 3 July 2021

Table 1
High-speed machining (HSM) parameters.

Parameter	Value
Cutting speed (m/min)	314
Radial cutting depth, a_e (mm)	0.20
Axial cutting depth, a_p (mm)	0.15
Feed per tooth, f_z (mm)	0.18
Cutting tool rotation (rpm)	30,000
Medium	Air

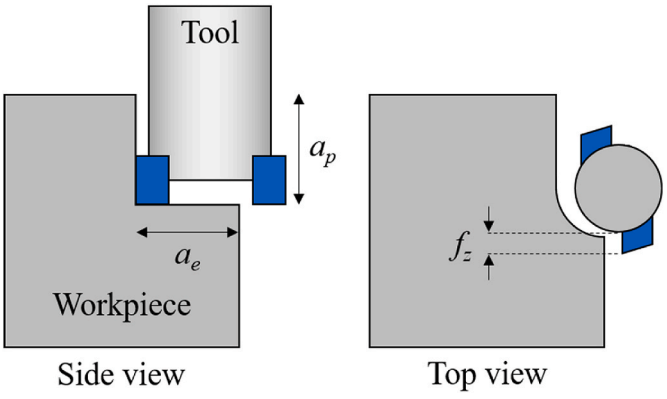

Fig. 1. Schematic diagram of the HSM procedure.

Table 2
Clean up procedure applied to t-EBSD datasets (OIM Analysis™ 5.2).

Clean-up procedure	Parameters
Grain dilation	Grain tolerance angle: 15° Minimum grain size: 10 points
Neighbour CI correlation	Minimum confidence index: 0.1

processes. This is considered to be constituted by three steps: shaping, debinding and sintering. It must be highlighted that such processing is now one of the most common.

Consequently, the chips generated by HSM of as-quenched tool-steel dies/moulds, may originate in AM parts/components new microstructures with high performance. Steel powders for AM are typically produced by atomisation, which can be further processed through ball-milling to produce a nanocrystalline powder structure [3,4] with superior mechanical properties [5,6]. In a previous approach, it was characterised AISI-SAE H13 tool-steel chips generated by conventional machining procedures [7]. Using the chips generated by HSM tool-steel dies/moulds for powder production is a very appealing idea because it merges an energy-efficient recycling method of industrial wastes, with an energy-efficient powder fabrication route, avoiding the high cost associated with atomisation. However, this innovative recycling route for hardened tool-steel chips is still underexplored. The present study is a part of an arrangement to evaluate the aforementioned solid-state recycling route to produce powder for AM indirect processes, focusing on the mechanical and microstructural characterisation of chips generated by HSM of as-quenched tool-steel. Studying the microstructure of the chips is important because it does affect their mechanical properties, their response to the milling process, and the quality of the resulting powder. The quality of the powder, namely its microstructural features, will have a strong influence on the mechanical behaviour of the succeeding parts/components produced by AM.

2. Materials and methods

2.1. HSM of AISI-SAE H13 tool-steel

Steel chips were generated from HSM of as-quenched AISI-SAE H13 tool-steel (X40CrMoV5-1) in a MIKRON HPM 600U (GF Machining Solutions, Switzerland), whose cutting parameters are summarised in Table 1 and illustrated in Fig. 1. It is noteworthy that this machining procedure took place in a die/mould manufacturing industrial facility and the cutting parameters presented in Table 1 are part of common industrial HSM practices. This is essential to ensure that chip characteristics unveiled in this work are to a certain extent representative of the chips generated across the die/mould manufacturing industries.

2.2. Chip characterisation

Chips were collected having not received any further treatment/processing. Chip size, shape and surface morphology were evaluated by scanning electron microscopy (SEM) (Quanta 400 FEG, FEI Company, USA) at 15 keV. Chips were embedded in epoxy resin, ground in sandpaper and fine-polished in 6 and 1 μm diamond suspension for Vickers microhardness indentation tests (Duramin, Struers, Denmark), with a load of 50 g and 10 indentations per specimen. Phase identification was performed by X-ray diffraction, XRD (XPert PRO, PANalytical, Netherlands) with Bragg-Brentano geometry, Cu Kα radiation ($\lambda = 0.15406$ nm) with a step of 0.04°, and a voltage and current intensity of 45 kV and 40 mA, respectively. Cross sectional thin foils were extracted from two chip regions by focused ion beam, FIB (Helios Nanolab, FEI Company). The thin foils were thinned down at 5 kV for transmission electron microscopy, TEM (Tecnai G^2 F20, FEI Company) at 200 kV and

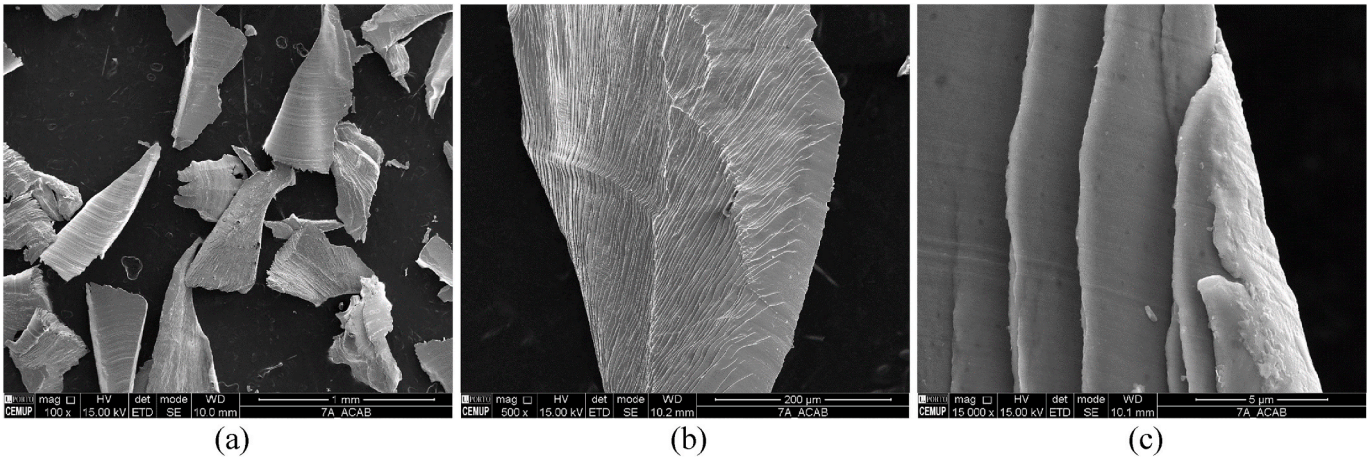

Fig. 2. As-machined chips (a), ASB at the free surface of the chip (b) and respective detail (c) by SEM.

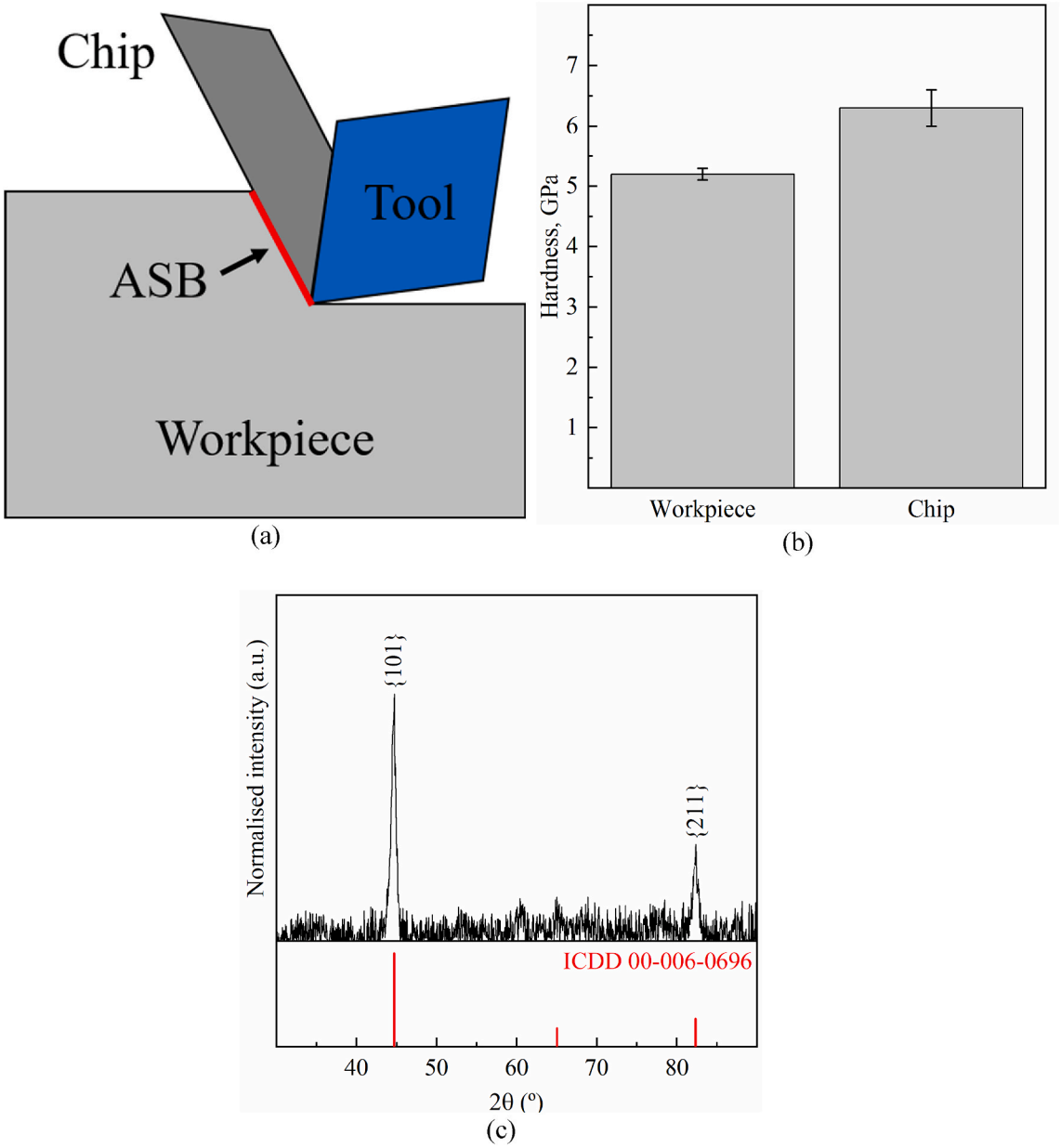

Fig. 3. Schematic diagram of the ASB location (a), hardness of the chip and workpiece (as-quenched) (b), and XRD of the chips (b).

for transmission electron backscattering diffraction mapping, t-EBSD (EDAX). The thin foils were positioned at a 27° angle tilt relative to beam normal and data were collected with a 10 nm step on a hexagonal grid configuration. Total area analysed was 1.2 × 1.2 μm^2. t-EBSD datasets were processed in OIM Analysis™ 5.2 according to the procedure in Table 2.

3. Results and discussion

3.1. Chip morphology, hardness, and structure

HSM of as-quenched AISI-SAE H13 tool–steel workpiece results in small sized chips (Fig. 2a), approximately 1 mm long and 0.7 mm wide. At high cutting speeds, the tool tip imposes high strain rates to the surface of the workpiece, causing chip extraction to be assisted by repeated adiabatic shearing [8] where intense material flow occurs. The occurrence of these highly strained regions, adiabatic shear bands (ASB), increases with cutting speed and are characteristic of HSM chips, leaving a fine saw teeth-like shape on the free surface of the chip (Fig. 2b and c) [9]. ASB is developed between the tip of the cutting tool and the chip free surface (Fig. 3a). The effect of localised conditions in HSM, between the chip and the cutting tool on the chip microstructure, will be highlighted afterwards. Chip microhardness increases 21%, from 5.2 ± 0.1 (workpiece) to 6.3 ± 0.3 GPa (chip) (Fig. 3b). The bcc/bct martensite (Fe-α') is the only phase detected by XRD (Fig. 3c), with similar crystal structure as bcc ferrite (ICDD 00-006-0696). Martensite in steels with C content inferior to 0.4 wt% displays a lattice parameter ratio c/a = 1 [10], which means low carbon.

3.2. TEM microstructural characterisation

TEM analysis reveals two distinct microstructures inside ASB. FIB thin foil (F1), adjacent to the ASB, exhibits a dispersion of carbide particles in an elongated grain matrix (Fig. 4a). The indexed diffraction pattern (DP) of the carbides correspond to fcc structure of V_xC_y [11]. Dark field (DF) micrographs allow a better visualisation of such

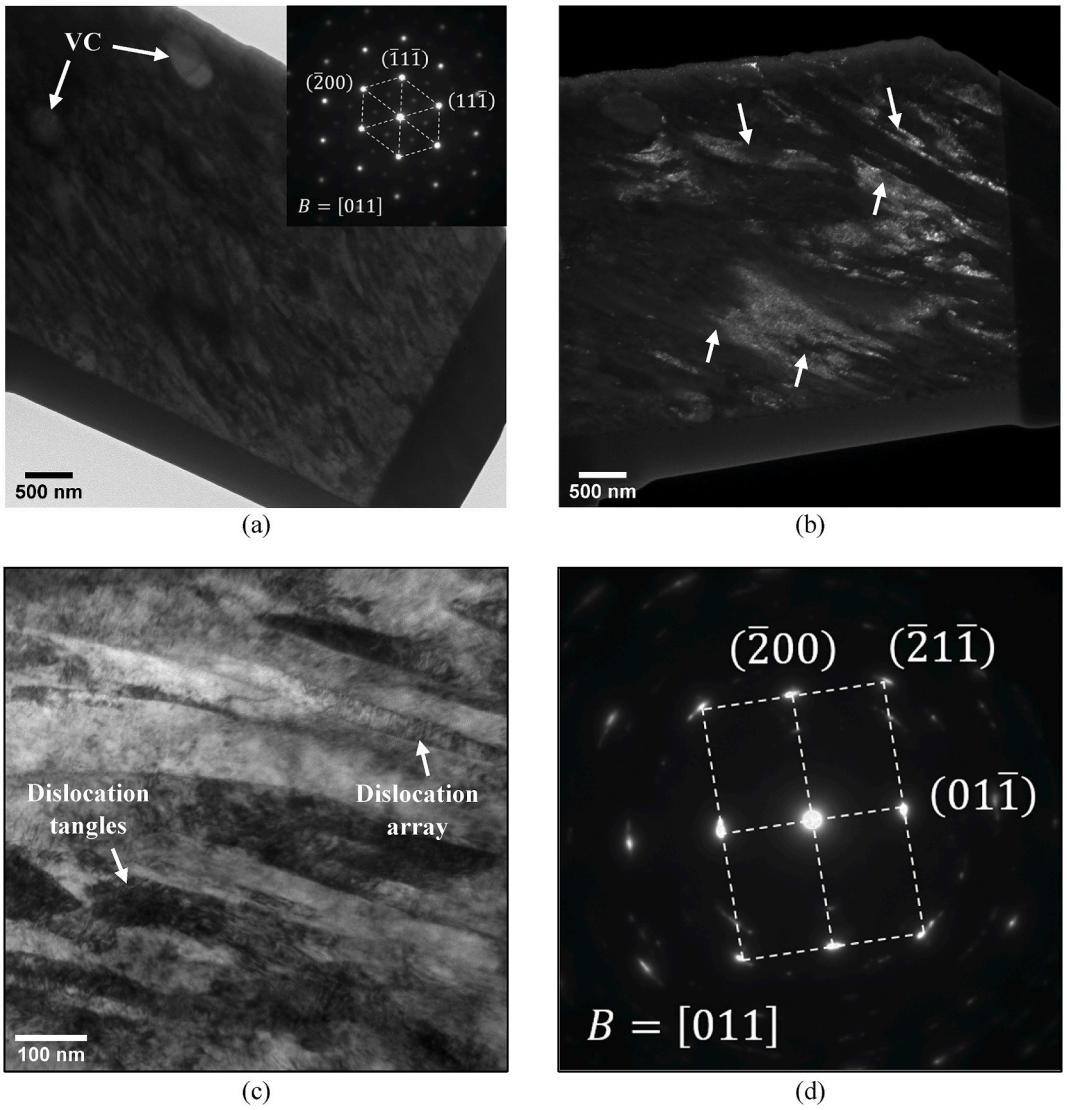

Fig. 4. BF (a) and DF (b) TEM images of specimen L1; strained martensite laths (c) and corresponding SAED pattern (d).

elongated grain structure and the extension of the strain across the lamella (Fig. 4b). Bright zones represent specific crystal orientations given by electron diffraction to a particular area in the TEM back focal plane, which was selected to acquire this micrograph. Unstrained grains, with specific crystal orientations relative to the incident electron beam, *B*, either appear bright or dark in DF imaging, depending on whether diffracted electron beams are allowed through the back focal plane or not. In this case, however, individual grains display both, bright and dark zones, indicating that several orientations are present within a single grain (white arrows in Fig. 4b). Duan and Zhang [9] described such inner grain structure appearance mechanism in HSM of quenched and tempered AISI-SAE 1045 carbon steel. In ASB formation conditions, the dislocation density increases steeply, forcing grain reorientation in the direction of the plastic flow. As the strain accumulates, the transient temperature that develops inside ASB and at the chip-tool triggers dislocation climb and dislocation cell formation, eventually resulting in sub-grain/low angle grain boundaries (LAGB) that change the angle of electron diffraction [12,13]. Fig. 4c reveals dislocation arrays and tangles within elongated martensite laths, some <100 nm thick, substantially misoriented, one relative to another [14]. This is seen in the corresponding selected area electron diffraction (SAED) pattern, where significant in-plane rotations along direction [011] are visible (Fig. 4d) [15]. The second FIB thin foil (F2), near the centre of ASB, displays a discontinuous martensite lath microstructure (Fig. 5a), which is more evident in DF imaging (Fig. 5b). As the strain accumulates further, sub-grain misorientation increases, giving origin to LAGB and high angle grain boundaries (HAGB), favouring segmentation of the martensitic laths (Fig. 5c). These segments display a near-equiaxed grain shape and a high misorientation angle, one relative to another, and grain regions with high dislocation density. SAED obtained on Fig. 5c produces a ring pattern, compatible with a randomly oriented, nanocrystalline microstructure (Fig. 5d) [16].

3.3. *t-EBSD microstructural characterisation*

Inverse pole figure (IPF) maps obtained by t-EBSD are shown in Fig. 6a and b after cleaning up the dataset according to Table 2. Fig. 6a depicts the elongated grain structure of L1 formed by adiabatic shear in the chip, and reveals the starting stage of martensite lath segmentation, which is not easily observed by TEM. The colour in IPF mapping represents crystal orientation. Sub-grain boundaries between 3-5° are highlighted as blue lines (Fig. 6c and d). Broken red arrows point to the LAGB (5–15°) that arise from dislocation build-up and climb from sub-grain regions, acting as precursors of HAGB (>15°) for higher levels of strain [17]. In such cases, when the LAGB convert to HAGB, the precursor sub–grain cells become independent grains (dark arrow). As the

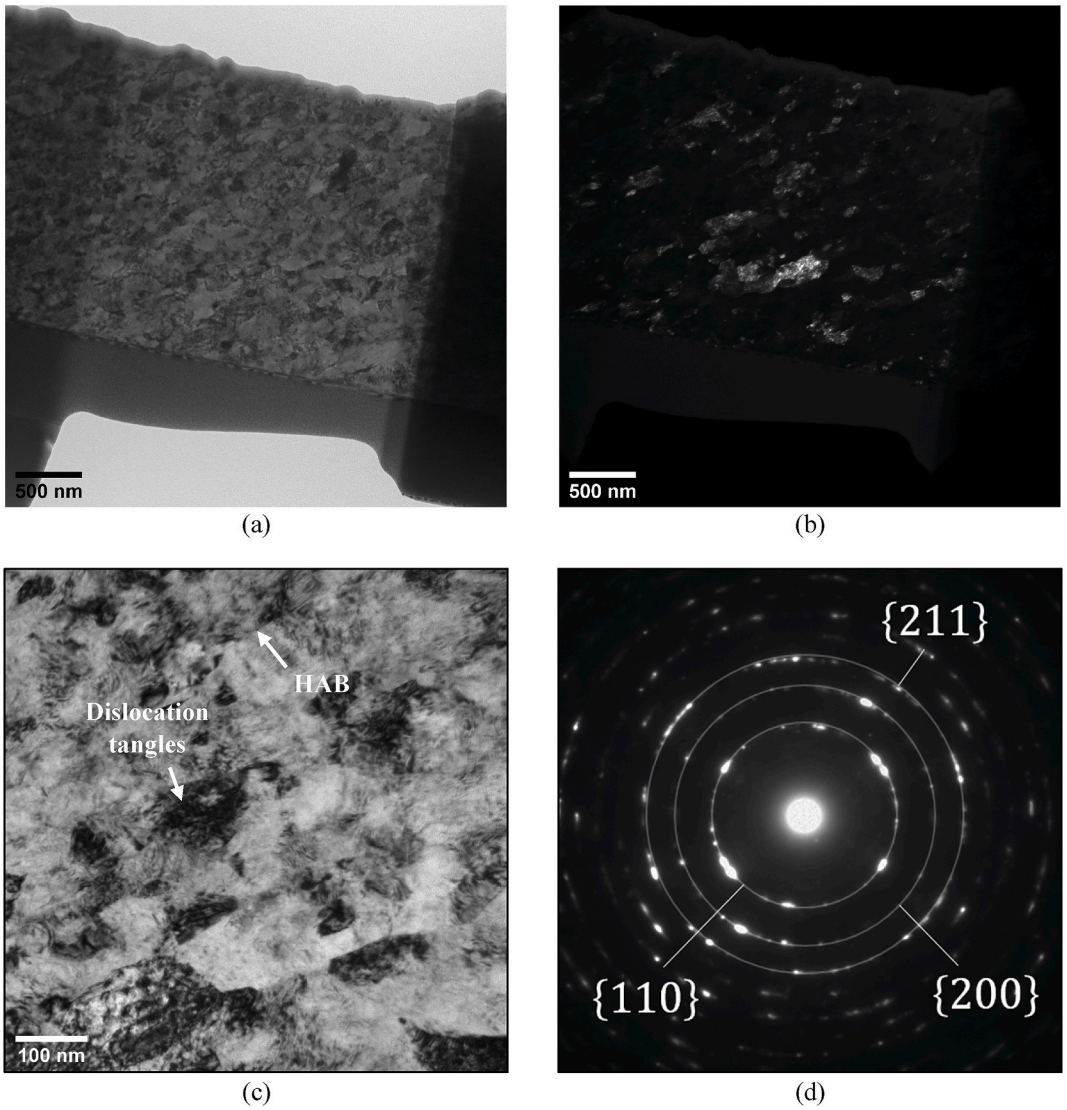

Fig. 5. BF (a) and DF (b) TEM images of specimen L2; near-equiaxed martensitic grain (c) and corresponding SAED pattern (d).

plastic flow near the centre of the ASB increases and additional strain accumulates, extensive martensite lath segmentation is observed (Fig. 6b). The elongated structures are progressively shortened as more sub-grain cells accumulate crystal misorientation relative to their neighbours, evolving to HAGB. Under such high strain rate conditions, the transient temperature developed near the centre of ASB is assumed to be sufficiently high to initiate recrystallisation, causing the sub-grain cells to separate from the lath in the direction of shearing, emerging as small, near-equiaxed grains, separated by HAGB. Heat transfer from the centre of ASB to the surrounding areas, imposes a fast rate of cooling below the recrystallisation temperature, preventing grain growth. This grain-refining mechanism is responsible for a nanocrystalline/ultrafine grain structure with average grain size $\overline{d} = 85$ nm (Fig. 7) inside ASB. Thus, chip hardening, relative to the workpiece, can be explained by a combination of highly strained regions in the surrounding areas of ASB and by a grain-refining effect that is a direct consequence of intensive strain build-up followed by localised recrystallisation. Therefore, chips generated by HSM of as-quenched tool-steel dies/moulds display interesting properties as superior raw materials for the fabrication of nanocrystalline steel powder, combining high hardness with partial nanometric grain structure. Chip grinding into powder is a promising solid-state recycling approach for these type of industrial wastes. Evidently, the conversion of the chips into powder for AM, as well as powder structure and morphology, are further steps required to validate the proposed approach, which will be addressed in future works.

4. Conclusions

The microstructure of ASB in AISI-SAE H13 tool–steel chips generated by HSM was studied by SEM, XRD, TEM and t-EBSD. The chips display a bcc/bct martensitic phase with a fine dispersion of V_xC_y with increased hardness relative to the as-quenched workpiece. The regions adjacent to the ASB are characterised by thin martensite laths with high dislocation density and the formation of sub-grain boundaries. The microstructure inside the ASB consists of ultrafine and nanocrystalline grains. t-EBSD mapping demonstrates the grain-refining mechanism that is mediated by progressive martensite lath segmentation into smaller, near-equiaxed grains. This grain-refining mechanism is activated by the intense plastic flow of material and transient localised temperature that initiates recrystallisation on the highly strained regions. Although chips generated by HSM of AISI-SAE H13 tool–steel do not exhibit homogeneous microstructure, their hardness and partial nanocrystallinity make them promising high quality raw material for nanocrystalline powder production to supply indirect additive manufacturing processes.

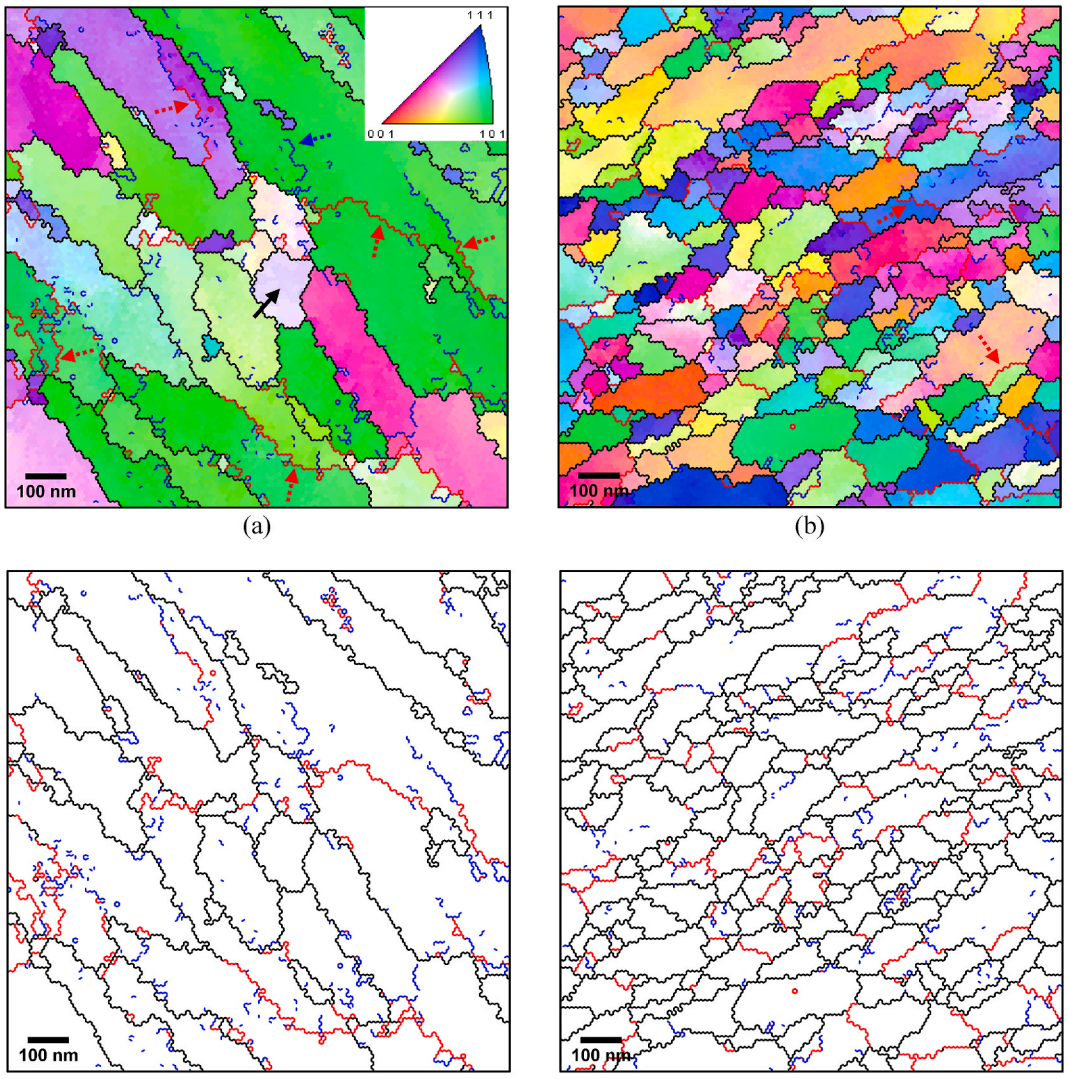

Fig. 6. IPF maps of specimens F1 (a) and F2 (b) by t-EBSD. HAGB (15-180°), dark lines, LAGB (5-15°), red lines, and sub-grain boundaries, blue lines, are highlighted in (c) and (d), respectively. (For interpretation of the references to colour in this figure legend, the reader is referred to the Web version of this article.)

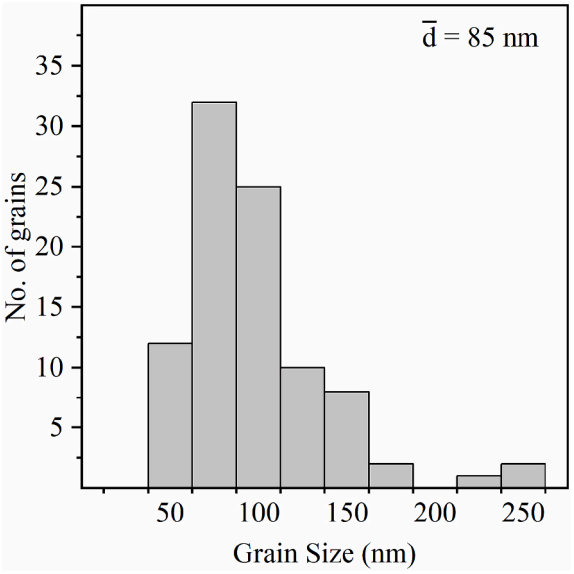

Fig. 7. Grain size distribution from t-EBSD mapping of specimen L2 (excluding grains intersecting map edge).

Author statement

R.F. Santos: Methodology, Formal analysis, Investigation, Writing – original draft, Visualisation. A.R. Farinha: Investigation. R. Rocha: Investigation, C. Batista: Investigation. C. Costa Rodrigues: Project administration, Funding acquisition. M.T. Vieira: Conceptualization, Writing – review & editing, Supervision, Project administration, Funding acquisition.

Declaration of competing interest

The authors declare that they have no known competing financial interests or personal relationships that could have appeared to influence the work reported in this paper.

Acknowledgments

This work was supported by FEDER funds through COMPETE, Programa Operacional Factores de Competividade, Add.Additive – Add Additive Manufacturing to Portuguese Industry (grant number POCI–01-0247-FEDER-024533), Add.Powder (grant number 39910), national funds provided by FCT, Fundação para a Ciência e a Tecnologia, (grant numbers UIDB/00285/2020 and UIDB/04044/2020), Centro2020 through PAMI–ROTEIRO/0328/2013 (no. 022158), and by project

QREN MaisCentro MT4MOBI – Materials and Technologies for Greener Manufacturing & Products Applied to Mobility.

References

[1] S. Chinchanikar, S.K. Choudhury, Machining of hardened steel – experimental investigations, performance modelling and cooling techniques: a review, Int. J. Mach. Tool Manufact. 89 (2015) 95–109, https://doi.org/10.1016/j.ijmachtools.2014.11.002.

[2] G. Bhatta, L. Valladares, X. Liu, Z. Ma, A.B. Domínguez, N.O. Moreno, S.E. Suarez, C.H.W. Barnes, D. Zhang, Microstructure and mechanical properties of solid state recycled 4Cr5MoSiV (H11) steel prepared by powder metallurgy, Res. Mater. (2021) 100184, https://doi.org/10.1016/j.rinma.2021.100184.

[3] G.V. Thotakura, R. Goswami, T.V. Jayaraman, Structure and magnetic properties of milled maraging steel powders, Powder Technol. 360 (2020) 80–95, https://doi.org/10.1016/j.powtec.2019.09.054.

[4] L. Heidari, M.J. Hadianfard, A.R. Khalifeh, D. Vashaee, L. Tayebi, Fabrication of nanocrystalline austenitic stainless steel with superior strength and ductility via binder assisted extrusion method, Powder Technol. 379 (2021) 38–48, https://doi.org/10.1016/j.powtec.2020.10.028.

[5] E.N. Hahn, M.A. Meyers, Grain-size dependent mechanical behavior of nanocrystalline metals, Mat. Sci. Eng. A-Struct. 646 (2015) 101–134, https://doi.org/10.1016/j.msea.2015.07.075.

[6] F. Yin, G.J. Cheng, R. Xu, K. Zhao, Q. Li, J. Jian, S. Hu, S. Sun, L. An, Q. Han, Ultrastrong nanocrystalline stainless steel and its Hall-Petch relationship in the nanoscale, Scripta Mater. 155 (2018) 26–31, https://doi.org/10.1016/j.scriptamat.2018.06.014.

[7] S.C. Godinho, R.F. Santos, M.T. Vieira, In the search of nanocrystallinity in tool-steel chips, Sci. Technol. Mater. 29 (1) (2017) e62–e67, https://doi.org/10.1016/j.ctmat.2016.07.016.

[8] G.G. Ye, S.F. Xue, W. Ma, M.Q. Jiang, Z. Ling, X.H. Tong, L.H. Dai, Cutting AISI 1045 steel at very high speeds, Int. J. Refract. Met. H. 56 (2012) 1–9, https://doi.org/10.1016/j.ijmachtools.2011.12.009.

[9] C.Z. Duan, L.C. Zhang, Adiabatic shear banding in AISI 1045 steel during high speed machining: mechanisms of microstructural evolution, Mat. Sci. Eng. A-Struct. 532 (2012) 111–119, https://doi.org/10.1016/j.msea.2011.10.071.

[10] O.D. Sherby, J. Wadsworth, D.R. Lesuer, C.K. Syn, Revisiting the structure of martensite in iron-carbon steels, Mater. Trans. 49 (9) (2008) 2016–2027, https://doi.org/10.2320/matertrans.MRA2007338.

[11] T. Epicier, D. Acevedo, M. Perez, Crystallographic structure of vanadium carbide precipitates in a model Fe-C-V steel, Philos. Mag. A 88 (1) (2008) 31–45, https://doi.org/10.1080/14786430701753816.

[12] R.D.K. Misra, Z. Zhang, P.K.C. Venkatasurya, M.C. Somani, L.P. Karjalainen, Martensite shear phase reversion-induced nanograined/ultrafine-grained Fe–16Cr–10Ni alloy: the effect of interstitial alloying elements and degree of austenite stability on phase reversion, Mat. Sci. Eng. A-Struct. 527 (2010) 7779–7792, https://doi.org/10.1016/j.msea.2010.08.051.

[13] J.M. Longbottom, J.D. Lanham, A review of research related to Salomon's hypothesis on cutting speeds and temperatures, Int. J. Mach. Tool Manufact. 46 (2006) 1740–1747, https://doi.org/10.1016/j.ijmachtools.2005.12.001.

[14] D. Panov, O. Dedyulina, D. Shaysultanov, N. Stepanov, S. Zherebtsov, G. Salishchev, Mechanisms of grain structure evolution in a quenched medium carbon steel during warm deformation, Crystals 10 (7–554) (2020) 1–16, https://doi.org/10.3390/cryst10070554.

[15] Y. Xiong, Y. Yue, Y. Lu, T. He, M. Fan, F. Ren, W. Cao, Cryorolling impacts on microstructure and mechanical properties of AISI 316 LN austenitic stainless steel, Mat. Sci. Eng. A-Struct. 709 (2018) 270–276, https://doi.org/10.1016/j.msea.2017.10.067.

[16] B. Li, S. Zhang, Y. Fang, J. Zhang, Z. Liu, Deformation behaviour and texture evolution of martensite steel subject of hard milling, Mater. Char. 156 (2019) 109881, https://doi.org/10.1016/j.matchar.2019.109881.

[17] G. Faraji, H.S. Kim, H.T. Kashi, Severe Plastic Deformation: Methods, Processing and Properties, first ed., Elsevier Science Publishing Co Inc, United States, 2018.